Design of Steel Columns at Elevated Temperatures Due to Fire: Effects of Rotational Restraints

ANIL AGARWAL and AMIT H. VARMA

ABSTRACT

The stability of steel building structures under fire loading is often governed by the performance of the gravity load resisting systems. The inelastic buckling failure of gravity load bearing columns can potentially initiate and propagate stability failure of the associated subsystem, compartment or story. This paper presents a design methodology for wide-flange hot-rolled steel columns (W-shape) under uniform compression at elevated temperatures. A number of simply supported W-shape columns were modeled and analyzed using the finite element method (FEM). The analysis for axial loading followed by thermal loading was conducted using the nonlinear implicit dynamic analysis method to achieve complete stability failure. The models and analysis approach were validated using the results of existing column test data at elevated temperatures. The analytical approach was used to expand the database and to conduct parametric studies. The results are compared to existing column design equations at elevated temperatures and are used to propose revisions to the AISC ambient temperature design equations for steel columns to account for the effects of elevated temperatures and rotational restraints from cooler columns above and below the heated story.

Keywords: fire, elevated temperatures, steel column, design equation, FEM.

The fire safety of steel structures can be achieved by following the prescriptive fire-resistant design provisions recommended by building codes such as the IBC (ICC, 2009) or NFPA 5000 (NFPA, 2009). A fire-resistant design is achieved by selecting individual structural components (columns, beams, floor assemblies, etc.) with a design fire-resistance rating (FRR) greater than or equal to the required or prescribed FRR. The required FRR values are prescribed by building codes based on building geometry, use and occupancy. The design FRR values are determined by conducting standard fire tests in accordance with ASTM E119 (ASTM, 2008a) or by standard calculation methods based on previous ASTM E119 test results available in AISC *Steel Design Guide 19* (Ruddy et al., 2003), ASCE/SEI/SFPE 29-05 (ASCE, 2005), or IBC.

The prescriptive design approach is rooted in the ASTM E119 fire test and has some deficiencies that are identified and discussed in AISC *Steel Design Guide 19* and Beyler et al. (2007). The standard fire test does not account for the interaction among various components of the structural system exposed to fire. The fire time-temperature (*T*-*t*) curves used in the standard tests are somewhat idealistic and may not represent realistic fire scenarios. These deficiencies, along with the need for structural performance–based design guidelines for fire safety, have been highlighted by recent investigation reports on the World Trade Center towers and World Trade Center-7 (WTC-7) building collapses in the NIST NCSTAR 1-9 (NIST, 2008). In order to develop structural performance–based fire resistance design guidelines there is a need to understand the behavior of individual components at elevated temperatures and their structural interaction with other surrounding cooler components.

Recent research by Usmani (2005), Varma et al. (2008) and the National Institute for Standards and Technology (NIST) has indicated that the overall behavior and stability of building structures under fire loading depends on the performance of the gravity-load-bearing systems, including the floor system, associated connections and gravity columns. In a compartment fire, gravity columns can lose stability for two reasons: (1) an increase in column temperature can reduce its stiffness and strength, and (2) the expansion and contraction of beams can produce large deformation demands in the connections. Failure of these connections can render gravity columns unbraced for more than one story. In either case, developing an understanding of the failure behavior of compression members at elevated temperatures is crucial for evaluating the overall safety of a structure.

A column in a compartment fire is not an isolated member. Gravity columns of multistory buildings are typically continuous over three stories (36 to 40 ft) and braced at each story level. During a story-level fire event, the gravity columns in the heated story may experience rotational restraints from the cooler columns above and below and axial restraints against thermal expansion due to the surrounding structure. These restraints can alter both the load demand

Anil Agarwal, Graduate Research Assistant, School of Civil Engineering, Purdue University, West Lafayette, IN. E-mail: anilagar001@gmail.com

Amit H. Varma, Associate Professor, School of Civil Engineering, Purdue University, West Lafayette, IN. E-mail: ahvarma@purdue.edu

on the column and its axial load capacity, which should be considered in the analysis and design process.

There has been a significant amount of research on the behavior of steel compression members at elevated temperatures. Over past few decades, researchers such as Olesen (1980), Vandamme and Janss (1981), Aasen (1985), Janss and Minne (1981) and Franssen et al. (1998) have conducted a large number of fire tests on steel columns; therefore, a large database exists for elevated temperature tests conducted on simply supported columns. Most of these tests, however, were conducted on very small and slender column members. In some research (e.g., Lie and Almand, 1990), there was uncertainty about end fixity achieved by the test boundary conditions. In other research (e.g., Aasen, 1985), the temperature variability was so high that analytical simulation was very difficult. Considering the complexity of conducting large-scale fire tests on steel columns, there is a significant need for analytical models and tools that can predict the behavior of steel columns subjected to fire loading.

Analytical methodologies or tools and empirical equations for design have been developed by many researchers to estimate the response of structural systems or individual members under fire conditions. Several commercially available general-purpose programs are available, including ABAQUS (2009), ANSYS (2004) and LS-DYNA (2003). SAFIR (Franssen, 2005) from the University of Liege, Belgium, is also a popular finite element method (FEM)-based software designed particularly for nonlinear analysis of structures under fire. Hong and Varma (2009) along with Poh and Bennetts (1995a and 1995b) have developed fiber-based approaches to determine the stability behavior and inelastic buckling failure of compression members subjected to fire loading. The member analysis was done using a modified Newmark column analysis approach.

Talamona et al. (1997) used the results of numerical parametric studies and experimental data to develop and validate a set of design equations for calculating the buckling strengths of simply supported steel columns at elevated temperatures. These design equations are part of Eurocode 3 (EN, 2005) design guidelines, and they use Eurocode 3 prescribed steel stress-strain-temperature (σ-ε-T) curves at elevated temperatures. AISC 360-05 (AISC, 2005a) provides a simpler table, based on the Eurocode 3 σ-ε-T curves, for calculating the elastic modulus and yield stress values at various elevated temperatures. The AISC 360-05 specification recommends the use of the ambient temperature column design equations with modified material properties given in the table mentioned earlier for elevated temperatures. However, Takagi and Deierlein (2007) have shown this approach to be highly unconservative. They used ABAQUS to develop and analyze finite element models of wide-flange steel columns under fire loading and to conduct parametric studies on these columns. They used the Eurocode 3 material σ-ε-T relationships at elevated temperatures for the models and developed design equations using the results from the parametric study. The design equations developed by Takagi and Deierlein have a different format from AISC column design equations at ambient temperature. These equations are calibrated to the Eurocode 3 σ-ε-T curves for steel and would need to be revised if any other material model (e.g., the material model developed by NIST NCSTAR 1-9 for WTC-7 steel) is to be used. Additionally, these equations are limited to columns with simply supported boundary conditions.

At elevated temperatures, surrounding members may restrain the heated steel columns against displacement and rotation at the ends. The presence of restraints against thermal expansion may induce additional loads, which may force an early failure of the column, whereas the continuity of the column with other cooler members may enhance its stability. Eurocode 3 accounts for the benefits of the rotational end restraints in a simple manner. It recommends using 50 and 70% of the actual unbraced length as effective length for columns continuous at both ends and at one end, respectively. Valente and Neves (1999) used an FEM-based software to evaluate the behavior of the columns that are restrained against thermal expansion and end-rotation under fire condition. They used Euler-Bernoulli beam elements to model the columns and linear-elastic springs to model the restraints. They concluded that the Eurocode 3 recommendation is appropriate only for short columns with very high rotational restraints offered by the neighboring frame elements. However, Valente and Neves did not provide any comprehensive guidelines for calculating the beneficial effects of rotational restraints on the columns under fire loading.

Using experiments and numerical techniques, Rodrigues et al. (2000), and Neves at al. (2002) developed an empirical relationship between failure temperatures of a column that is free to elongate an axially restrained column. The experimental study was conducted on small-scale steel bars of diameter varying between 5 and 20 mm and slenderness values varying between 80 and 319. The authors substantiated their conclusions through numerical parametric studies on real column sections. They drew two main conclusions: (1) the critical failure temperature of columns decreases with an increase in the stiffness of axial restraint—although beyond a particular value of the axial restraint stiffness, there is no further reduction in the critical temperature; and (2) the decrease in the critical temperature is greater for columns buckling (bending) about the weak axis. Wang and Davies (2003a, 2003b) tested several columns at elevated temperatures with one end restrained against thermal expansion and rotation. A continuous beam was used for the purpose of providing these restraints. The authors found that using 70% of the actual length predicts the column failure temperature quite reasonably.

In all the cases previously mentioned, the constraints are

assumed to have a constant spring stiffness that is independent of the axial load in the column. The rotational restraint provided by cooler columns above and below depends on their flexural stiffness, which depends significantly on their axial loading and stability limit or coefficient (Chen and Lui, 1987). Therefore, our hypothesis is that instead of analyzing or testing the effects of the restraints through rotational springs, a better approach would be to model the continuous column in its totality and to load the restraining (cooler) elements axially as they would be loaded in real structures.

This paper develops a new set of design equations for wide-flange hot-rolled steel columns at elevated temperatures. These equations have the same format as the AISC 360-05 column design equations at ambient temperatures. The paper also presents a simple modification to the elevated temperature column design equations to account for the beneficial effects of rotational restraints due to the continuity of the heated column with potentially cooler columns above and below. The finite element modeling and analysis approach used in this study along with its validation using standard fire test results reported by other researchers are presented first. This is followed by the results of parametric studies conducted to evaluate the effects of slenderness, elevated temperature and rotational restraints on column axial load capacity. The results from the parametric analyses are used to develop design equations for simply supported columns at elevated temperatures and then to further develop a simple modification to include the beneficial effects of rotational restraints.

MODELING, ANALYSIS AND VALIDATION

As discussed in the previous section, continuity with cooler column elements at the ends improves the stability behavior of the column at elevated temperatures. This paper studies the stability behavior of steel columns with three different boundary conditions: (1) simply supported, (2) continuous with cooler column at one end and (3) continuous with cooler columns on both ends. In all three cases, the columns are loaded with uniform axial compression.

For simplicity, most of the design equations assume temperatures to be uniform along the length and through the cross-section of the column. The effects of nonuniform temperature distributions in column cross-sections are currently being evaluated and the results will be presented in a later paper. In this paper, the columns are assumed to have uniform temperature distribution. Because the elevated temperatures are uniform, the heating of the columns in the presented simulations is time independent and not associated with any particular fire event.

Disassociating uniform temperatures from time is a reasonable assumption as long as the effects of creep are accounted for. The effects of creep are typically insignificant, but they become more predominant at temperatures greater than 500 ºC (932 ºF). The Eurocode σ-ε-T curves implicitly account for the effects of creep for heating rates between 2 ºC/min and 50 ºC/min (3.6 ºF/min and 90 ºF/min). In the absence of better information, almost all guidelines (e.g., Talamona et al., AISC 360-05 and Takagi and Deierlein) use the Eurocode σ-ε-T curves to implicitly include creep effects, and thus disassociate uniform temperature from time. A similar approach has been used in this paper.

The commercially available finite element–based software, ABAQUS, was used for this analysis. The analysis scheme involves two steps: (1) loading of the column with axial load and (2) increasing the temperature of the column until failure. The axial loading in the first step was applied statically. The temperature increase in the second step was applied using the dynamic implicit analysis method with Newton-Raphson iterations to capture the complete stability failure of the column.

Material and Geometric Modeling

Temperature-dependent multiaxial material models were used for the steel material of the column. These models provide temperature-dependent isotropic elastic behavior and inelastic behavior defined by the Von Mises yield surface and associated flow rule. The temperature-dependent uniaxial stress-strain (σ-ε-T) and thermal expansion (α-T) relationships required to completely define the multiaxial material models were specified based on the corresponding σ-ε-T and α-T relationships for steel provided by Eurocode 3.

Two different finite element modeling approaches were considered for the columns. In the first approach, the column lengths were modeled using several two-node beam (B33) elements. The B33 element in ABAQUS is a sophisticated beam element in three-dimensional space with six degrees of freedom at each end, 13 integration points through the cross-section and three integration points along the length. The beam element is capable of modeling the effects of axial load, moment and torsion. Additionally, the beam element can be used to account for both geometric and material nonlinearity as a function of elevated temperatures. In the second approach, the column cross-section and length were modeled using several four-node shell elements (S4R). These shell elements model thick shell behavior and reduce mathematically to discrete Kirchhoff elements with reducing plate thickness. The four-node shell elements have six degrees of freedom per node, at least five integration points through the thickness and one (reduced) integration point in the plan area for integration along the length and width. Using the first approach involving beam (B33) elements for modeling the steel column requires fewer finite elements and is computationally inexpensive.

Preliminary investigations were conducted to compare and evaluate the two finite element modeling approaches with beam (B33) and shell (S4R) elements. These

investigations indicated that the simpler model with beam (B33) elements is computationally efficient, but it has some major limitations. It cannot account for the effects of residual stresses, local buckling, and inelastic flexural torsional buckling in wide-flange columns. It cannot be used in a heat transfer analysis, but idealized *T-t* curve can be specified at maximum of five locations in the cross-section. This limitation is not relevant for uniform temperature analysis, but it is significant for cases with nonuniform heating. Modeling the column length and geometry with shell elements has the following advantages over beam elements. The shell element models can be used in a heat-transfer analysis and thus have more generalized temperature distribution. Residual stresses, local buckling and inelastic flexural torsional buckling can also be modeled reasonably. However, models using shell elements are computationally more expensive than the beam elements. Figures 1a and b show the deformed shapes of column buckling failure predicted using the beam element models and the shell element models, respectively. The deformed shape in Figure 1a is a three-dimensional rendering of the buckling failure mode predicted using beam (B33) elements. Comparing Figures 1a and b shows that local buckling effects can only be modeled using shell elements. The following subsections compare the results from analyses using both these modeling approaches in more detail.

Mesh Convergence

Refining the finite element mesh requires more computational resources but typically leads to more accurate results. In the case of models using beam elements, it is typically sufficient to use elements with length equal to the minimum of the depth and width of the column cross-section. According to this rule of thumb, eight equal-length beam elements should be sufficient to model the failure behavior of a 2.55-m (8.37-ft)-long W12×58 column. In a limited parametric study conducted on this column, it was observed that there is no significant difference in the failure temperatures predicted by models using 8 or 20 beam elements. Therefore, for all the further analyses, the length of each beam element is equal to the minimum of the depth and width of the column cross-section.

In the case of shell element models, using an unnecessarily large number of elements can consume a lot of computational resources; therefore, a more detailed parametric study was conducted to find the optimum number of elements required. A 2.55-m (8.37-ft)-long W12×58 column was

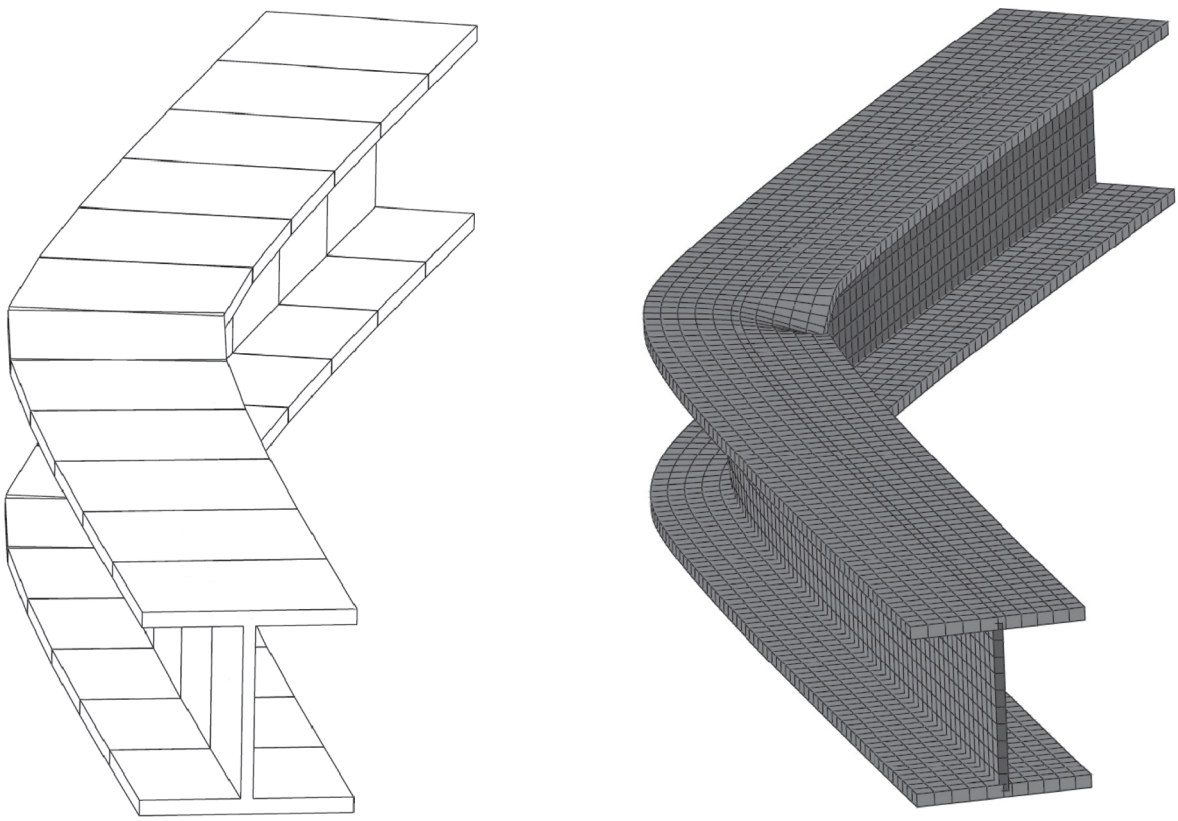

(a) (b)

Fig. 1. Rendered deformed shapes of the finite element models: (a) beam (B33) elements; (b) shell (S4R) elements.

analyzed with different levels of mesh refinements. Figure 2 shows how the predicted failure temperature of this column changes as the number of shell (S4R) elements used to model each flange and the web of the column changes from 2 to 12. Figure 2 also indicates that the failure temperature of columns can be predicted with 99% accuracy when six square-shaped S4R elements are used to model each flange and the web of the column cross-section. This was the mesh size and distribution used for all further work.

Residual Stress Effects

Residual stresses have significant influence on the axial load capacities of steel columns at ambient temperatures. Their influence on the column load capacity at elevated temperatures is investigated numerically using the shell element models. Residual stresses are introduced by assigning a nonuniform pseudo-temperature distribution through the column cross-section at a stress-free (unloaded) state and then changing these temperatures to the uniform ambient (20 ºC, 68 ºF) temperature. This process produces nonuniform thermal strains, which leads to nonuniform residual stresses through the cross-section as required (Ziemian, 2010). For example, Figures 3a and b show the initial and final pseudo-temperature distributions through a W12×58 column cross-section. The resulting residual stresses in the column after cooling to the ambient temperature are shown in Figure 3c. The initial pseudo-temperature distribution shown in Figure 3a was developed by trial-and-error procedure to produce maximum residual stress equal to 30% of the yield stress.

The effects of residual stresses on the failure temperatures of two different column sections were studied.

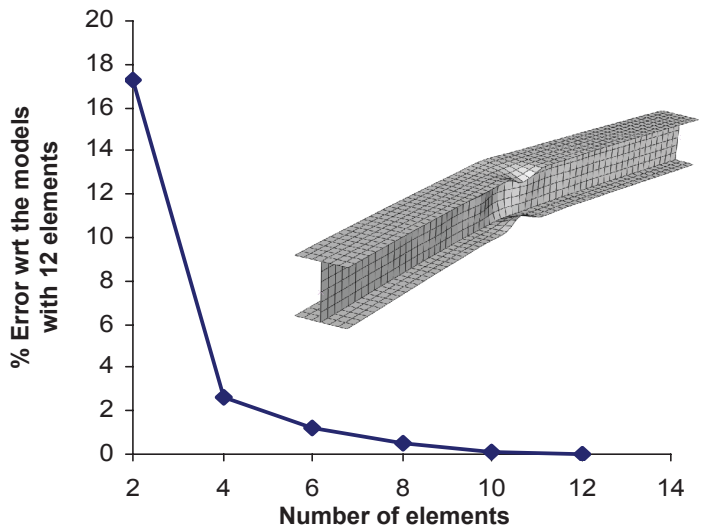

Fig. 2. Mesh convergence for shell (S4R) elements.

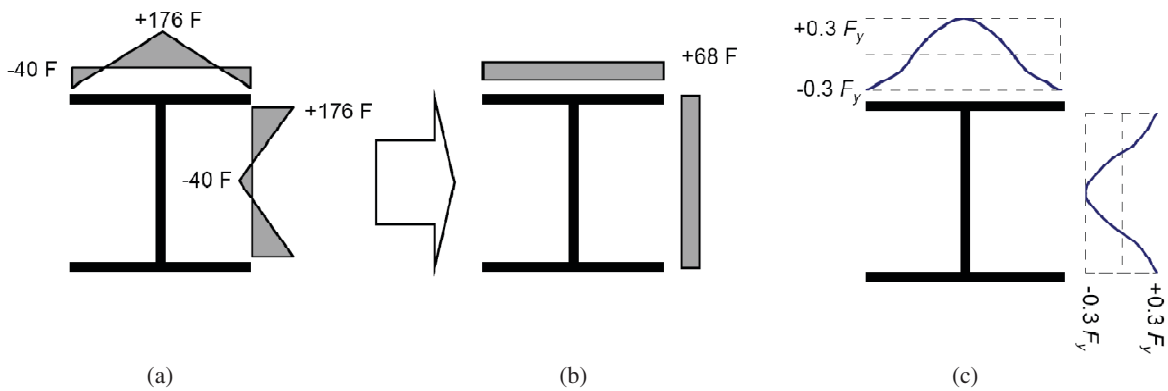

Fig. 3. Artificially assigned (a) initial and (b) final temperature distribution; (c) achieved residual stresses.

A 2.55-m (8.37-ft)-long W12×58 column (slenderness, L/r_y = 40) and a 4.12-m (13.52-ft)-long W8×35 (slenderness, L/r_y = 80) column subjected to various axial load values were analyzed to obtain the respective failure temperature values. Figure 4 shows that residual stresses have an influence on the column failure temperature; however this influence decreases as the column failure temperature increases. The effect of residual stresses on the column failure temperature cannot be ignored for failure temperatures less than about 500 ºC (932 ºF).

Initial Geometric Imperfection

The initial geometric imperfection for the wide-flange columns was developed by conducting elastic eigenvalue (buckling) analysis for the column with concentric axial loading. The buckling eigenmodes were used to define the shape of the geometric imperfection. The first two eigenmodes, i.e., the weak and strong axis flexural buckling modes, were both used to define the initial geometric imperfection in the column. The imperfection amplitude was assumed to be equal to the column length divided by 1500, based on the values measured and used at ambient temperatures (AISC, 2005a). The effects of local imperfection were also included by using the eigenmode corresponding to local buckling of the flanges and web to define an additional imperfection shape. The imperfection amplitude was assumed to be 1.6 mm (1⁄16 in.), which is the maximum permitted variation in section dimensions per ASTM A6 (ASTM, 2008b).

Validation

Both the beam and shell finite element models were used to predict the standard fire behavior and failure temperatures, T_F, of 29 wide-flange steel columns tested by Franssen et al. (1998). This database includes columns with a variety of cross-sections, nominal yield stresses, slenderness ratios and eccentricities. These columns had no fire protection and were tested by subjecting them to constant axial loading followed by a constant rate of heating. The reported experimental results included the failure temperatures, T_F, and the applied axial loading. Table 1 presents the comparison between the column failure temperatures observed in the tests, T_F (test), and the failure temperatures predicted by FEM simulations, T_F (S4R) and T_F (B33) for shell and beam elements, respectively. Yield strength, F_y, of the structural steel in the specimen ranged from 260 to 320 MPa (38 to 46 ksi).

Figure 5a shows comparisons of the failure temperatures predicted by the shell element models and those measured experimentally. As shown, the shell element models predict the failure temperatures with good accuracy. Similarly, Figure 5b shows comparisons of the failure temperatures predicted by the beam element models. The models with beam elements predict the failure temperatures with less accuracy than the models with shell elements. Additionally, the failure temperatures predicted by beam elements are slightly higher (unconservative) than the experimental results.

The shell element models were selected for conducting parametric studies on the simply supported columns. The simpler beam models were computationally efficient but not as accurate due to the limitations mentioned earlier. The primary limitation was the inability to model residual stresses and the local buckling distortions of the section flanges and webs. The beam element models will be more useful for modeling columns in large structural systems or where a member is expected to remain elastic, e.g., the cooler columns providing the end restraints to a heated column such

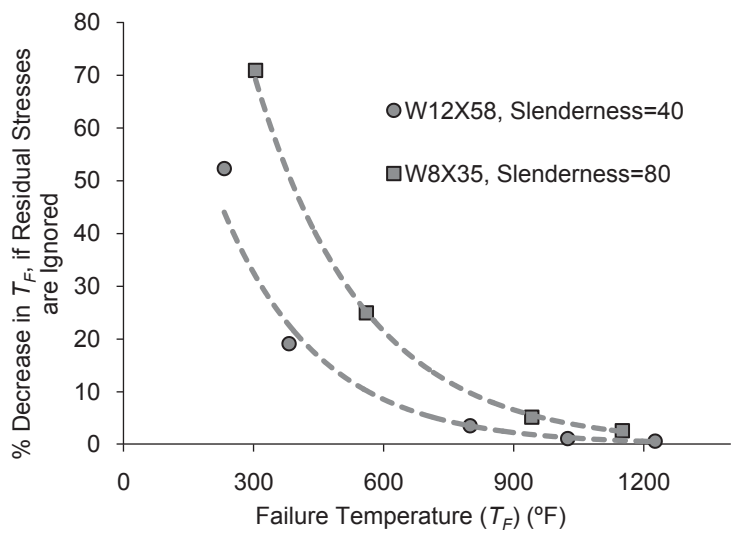

Fig. 4. Effect of residual stress on predicted failure temperature.

Table 1. Validation of the Shell (S4R) and Beam (B33) Elements Models against the Test Data										
Column	Length (in.)	P (kips)	e (in.)*	b_f (in.)	h (in.)	t_w (in.)	t_f (in.)	T_F (test) (°F)	T_F (S4R) (°F)†	T_F (B33) (°F)†
BL1	20.2	81.4	0.20 (W)	4.01	3.89	0.23	0.30	990	928 (–6.39)	894 (–9.96)
CL1	20.2	24.7	0.20 (W)	4.36	3.90	0.25	0.31	1281	1299 (–1.44)	1290 (0.72)
DL1	20.2	9.0	0.20 (W)	4.01	3.90	0.24	0.30	1585	1573 (–0.81)	1557 (–1.85)
BL3	50.1	65.6	0.20 (W)	4.03	3.89	0.24	0.30	734	748 (2.05)	716 (–2.56)
CL3	50.0	56.4	0.20 (W)	4.01	3.91	0.24	0.31	885	927 (4.85)	907 (2.53)
SL40	79.5	38.2	0.20 (W)	4.01	3.91	0.24	0.31	977	930 (–4.95)	961 (–1.71)
SL41	79.8	39.1	0.20 (W)	4.01	3.90	0.23	0.30	948	910 (–4.13)	918 (–3.34)
SL42	79.5	38.4	0.20 (W)	4.01	3.90	0.23	0.30	905	945 (4.54)	918 (1.44)
SL44	79.7	38.9	0.20 (W)	4.00	3.90	0.23	0.30	923	927 (0.40)	916 (-0.81)
AL5	109.1	28.5	0.20 (W)	4.01	3.90	0.23	0.30	855	892 (4.60)	997 (17.29)
BL5	109.1	16.4	0.20 (W)	4.01	3.90	0.23	0.30	1089	1105 (1.53)	1171 (7.84)
BL6	138.2	23.6	0.20 (W)	4.01	3.89	0.23	0.30	835	792 (–5.38)	991 (19.51)
CL6	138.2	20.2	0.20 (W)	4.02	3.90	0.23	0.30	919	975 (6.29)	1074 (17.44)
P1	157.5	22.5	3.94 (W)	7.88	7.93	0.36	0.59	1227	1225 (–0.15)	1261 (2.86)
P2	157.5	22.5	11.81 (W)	7.89	7.93	0.36	0.59	1067	1017 (–4.87)	1035 (–3.13)
P3	78.7	22.5	25.59 (S)	7.89	7.93	0.36	0.59	1110	1126 (1.50)	1139 (2.67)
P4	78.7	33.7	11.81 (W)	7.89	7.93	0.36	0.59	999	982 (–1.68)	986 (–1.30)
P5	78.7	22.5	9.84 (S)	6.43	7.09	0.55	0.89	1387	1344 (–3.19)	1350 (–2.79)
P6	196.9	22.5	19.69 (S)	6.44	7.10	0.55	0.89	1062	1054 (–0.70)	1105 (4.20)
P7	78.7	36.0	3.94 (S)	5.57	5.41	0.22	0.35	1002	1000 (–0.19)	1018 (1.67)
P8	196.9	22.5	3.94 (S)	5.50	5.27	0.22	0.33	945	882 (–6.90)	993 (5.33)

* W = failure about weak axis, S = failure about strong axis.
† Values in parentheses are percentage error with respect to the test data.

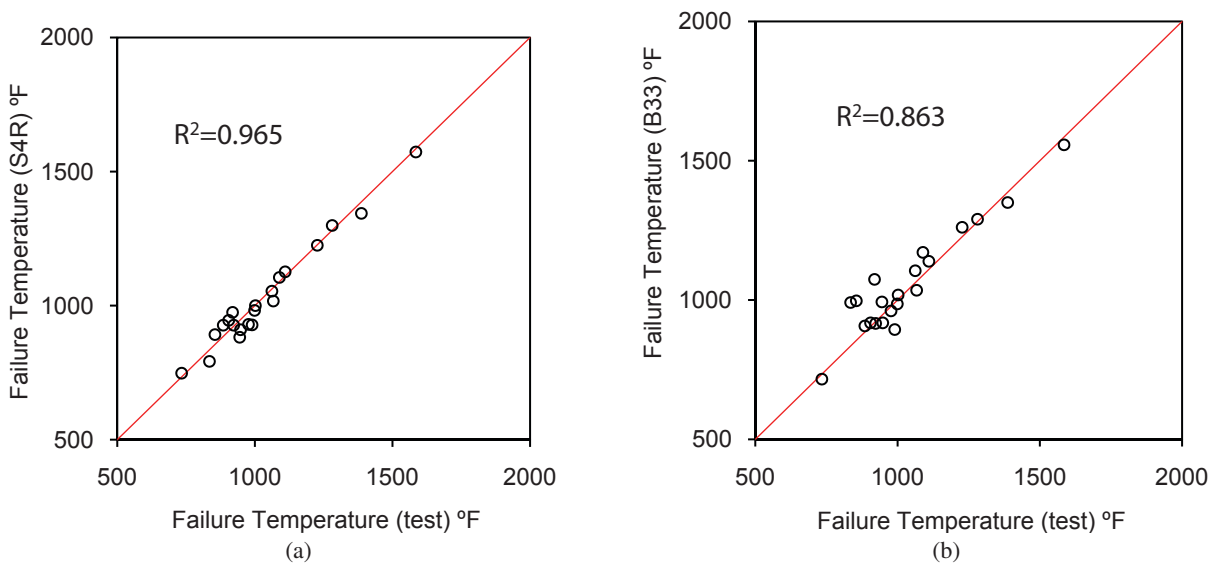

Fig. 5. Validation of structural analysis scheme against experimental data: (a) S4R elements; (b) B33 elements.

as the columns in the stories above and below the heated column.

PARAMETRIC STUDY AND RESULTS

The column capacity curves for W-shaped steel columns at elevated temperatures were developed using analytical data for a wide range of column dimensions, steel temperatures and column end conditions. The parametric studies were conducted on the following wide flange sections W8×35, W12×58, W14×90 and W14×159. These sections are commonly used for gravity columns in steel structures. The columns were assumed to be made from ASTM A992 (F_y = 50 ksi) structural steel. The results and guidelines presented in this paper are applicable for typical gravity column sections (weights between 35 and 160 lb/ft). Further evaluation may be required for large, heavy sections in the AISC *Steel Construction Manual* (AISC, 2005b) due to the presence of complex residual stresses in those sections.

Columns of each of the preceding four shapes were analyzed with (1) three different boundary conditions (simply supported, continuous at one end and continuous at both ends); (2) slenderness values ($\lambda = L/r_y$) ranging from 10 to 150; and (3) axial loads ranging from 20 to 100% of the ambient load capacity, P_n. For the case of simply supported boundary conditions, the column-ends were constrained to remain plane but were otherwise free to rotate in both horizontal directions. The finite element models for the cases of continuous columns were developed by modifying the models for simply supported columns by including the columns in the stories above and below, resulting in two-column or three-column subsystem models. The intermediate column was heated uniformly while the columns above and below remain at ambient temperature. Each of the columns in a two-column or three-column subsystem had the same length, cross-section and axial load level (P/P_n). This multicolumn subsystem is an idealization of the actual scenario, where the axial loads, lengths and sections can vary slightly.

The analysis was conducted using the validated finite element models. For the case of simply supported boundary conditions, the column was modeled using square-shaped four-noded shell (S4R) elements. These models used 19 nodes across the column cross-section and included the effects of residual stresses and global and local geometric imperfections. For the case of continuous columns, the columns above and below the heated column remain at ambient temperature and are not likely to fail before the heated column. These unheated columns were modeled using beam (B33) element models. The heated column was modeled using four-node shell (S4R) element similar to the model for simply supported columns.

Structural analysis was conducted by statically loading the columns to a preselected axial load level (20 to 100% of P_n) followed by uniform heating of the column under fire while analyzing the structural behavior using implicit dynamic analysis technique. All columns were observed to fail through inelastic buckling in the weak axis plane followed by local buckling of the flanges and webs as deformations increased. Tables 2, 3 and 4 summarize the failure temperatures for 64 W12×58 columns for the complete range of load levels (P/P_n), slenderness values and boundary conditions. The results shown in these tables indicate the failure temperature decreases with increasing axial load levels and that the failure temperature decreases with increasing slenderness for all slenderness values except when slenderness is greater than 80.

The results from Table 2 are presented graphically in Figure 6. This figure shows the plots of the normalized axial load capacities with respect to the failure temperatures for different slenderness values. The normalized axial load capacity is defined as the ratio of the axial load capacities at elevated and ambient temperatures. Figure 6 also includes the normalized material properties for structural steel (i.e., the yield stress, elastic modulus and proportionality limit) plotted against temperature. These normalized properties are the ratios of the corresponding material properties at elevated and ambient temperatures. The elevated temperature material properties were based on Eurocode 3 recommendations. The comparisons in Figure 6 indicate that:

- The reduction in the column axial load capacity is bounded by the reduction in the steel yield stress and the proportionality limit.
- The reduction in the axial load capacity of slender columns correlates with the reduction in the steel elastic modulus.
- The reduction in axial load capacity of shorter columns correlates with the reduction in the steel yield stress.

The reported failure temperatures were used to interpolate a three-dimensional surface relating the column slenderness, axial load level and failure temperatures. Figure 7 shows the interpolated three-dimensional surface for a W12×58 simply supported column, which was developed using MATLAB, a general-purpose mathematical software. Column capacity curves at a particular failure temperature or for a particular slenderness value can be obtained by taking longitudinal or transverse sections from this three-dimensional surface.

The values in Tables 2, 3, and 4 indicate that, as expected, the ambient load capacities, P_n, are not influenced by the end conditions. Continuity does not enhance the load capacity of a column at ambient temperatures because the columns above and below are also subjected to the same axial load and have the same length. However, the failure temperatures, T_F, corresponding to a particular slenderness value and axial loading, indicate that at elevated temperatures the

Table 2. Failure Temperatures from Parametric Studies on W12×58 Simply Supported Column								
W12×58		Failure Temperature (°F)						
λ_y	P_n (kips)	$0.9P_n$	$0.8P_n$	$0.7P_n$	$0.6P_n$	$0.5P_n$	$0.4P_n$	$0.2P_n$
10	840	509	824	918	988	1053	1125	1297
30	791	365	568	826	941	1013	1085	1267
40	726	360	513	725	892	986	1062	1254
50	659	360	502	657	831	963	1042	1238
60	601	340	466	615	775	943	1024	1220
80	486	333	453	572	705	882	1000	1202
100	380	333	462	568	685	862	999	1197
150	193	405	550	667	788	972	1047	1245

Table 3. Failure Temperatures from Parametric Studies on W12×58 Columns Continuous at Both Ends								
W12×58		Failure Temperature (°F)						
λ_y	P_n (kips)	$0.9P_n$	$0.8P_n$	$0.7P_n$	$0.6P_n$	$0.5P_n$	$0.4P_n$	$0.2P_n$
10	840	538	829	927	995	1062	1128	1303
30	827	550	842	936	999	1063	1125	1306
40	788	496	831	932	997	1063	1132	1308
50	743	471	795	916	990	1056	1128	1305
60	688	459	714	898	986	1054	1119	1299
80	544	448	682	891	993	1063	1135	1416
100	399	489	738	952	1029	1096	1171	1371
150	198	556	833	1015	1098	1171	1233	1465

Table 4. Failure Temperatures from Parametric Study on W12×58 Columns Continuous at One End								
W12×58		Failure Temperature (°F)						
λ_y	P_n (kips)	$0.9P_n$	$0.8P_n$	$0.7P_n$	$0.6P_n$	$0.5P_n$	$0.4P_n$	$0.2P_n$
10	840	552	835	927	993	1060	1126	1299
30	818	408	797	894	979	1051	1119	1294
40	770	403	657	864	961	1033	1101	1285
50	716	397	576	808	943	1017	1089	1276
60	654	392	556	756	912	1002	1078	1267
80	521	376	532	707	885	997	1074	1265
100	389	397	570	729	921	1018	1108	1281
150	197	478	657	838	995	1067	1139	1323

continuity with cooler columns increases the load capacity of the column significantly. The failure temperature for a column continuous at one end is higher than that of simply supported column. And, the failure temperature for a column continuous at both ends is higher than that of a column continuous at one end.

DESIGN EQUATIONS: SIMPLY SUPPORTED COLUMNS

As mentioned earlier, Takagi and Deierlein (2007) have proposed design equations for simply supported columns at elevated temperatures. These equations were also developed

based on the results of comprehensive three-dimensional finite element analysis. They compared well with the analytical results, but were discontinuous with the AISC column curves at ambient temperatures because they are in a different format. The Takagi and Deierlein equations form the basis of the 2010 AISC *Specification* (AISC 360-10).

This paper presents a modification to the AISC column curves at ambient temperatures so that they can also be used for elevated temperatures. The ambient temperature column curves were developed using elastic perfectly plastic stress-strain relationships for the steel material. This assumption does not hold at elevated temperatures because the stress-strain relationship has a significantly curved region between the proportional limit and the yield stress. Takagi and Deierlein (2007) have shown that the asymptotic bi-linearization of the curvilinear stress-strain curves—i.e., assuming the initial (or small-strain) slope as the effective elastic modulus, E^T, and the ultimate stress as the effective yield stress, $F_y{}^T$—leads to an unconservative estimate of the column capacity at elevated temperatures.

The curvilinear stress-strain curves at elevated temperatures, however, can be used to develop more appropriate equivalent elastic perfectly plastic stress-strain curves as described here and shown graphically in Figure 8a. The proof stress corresponding to 0.2% strain is taken as the equivalent yield stress, $F_y{}^T$. The equivalent elastic modulus, E^T, is selected by equalizing the area under the idealized elastic-plastic stress-strain curve and the actual curvilinear stress-strain curve. This involves numerical integration of the curvilinear stress-strain curve and some iterations to determine the equivalent elastic modulus. The equivalent elastic modulus and yield stress values corresponding to the Eurocode 3 steel σ-ε-T curves at elevated temperatures are calculated using preceding approach and are summarized in Table 5. Figure 8b shows a comparison between the equivalent steel property coefficients and Eurocode 3 steel property coefficients. As expected, the proposed equivalent coefficients are bounded by the corresponding Eurocode 3 values. These equivalent property values, E^T and $F_y{}^T$, can be used with the AISC column design equations shown in Equations 1, 2 and 3 to compute the axial load capacity, $P_n{}^T$, at elevated temperatures. In these equations, λ is the governing slenderness ratio equal to L/r_y, A is the cross-sectional area, and $F_e{}^T$ is the computed elevated temperature elastic buckling stress.

$$P_n^T = AF_y^T \left(0.658\right)^{\frac{F_y^T}{F_e^T}}, \qquad \text{if } F_e^T > 0.44F_y^T \tag{1}$$

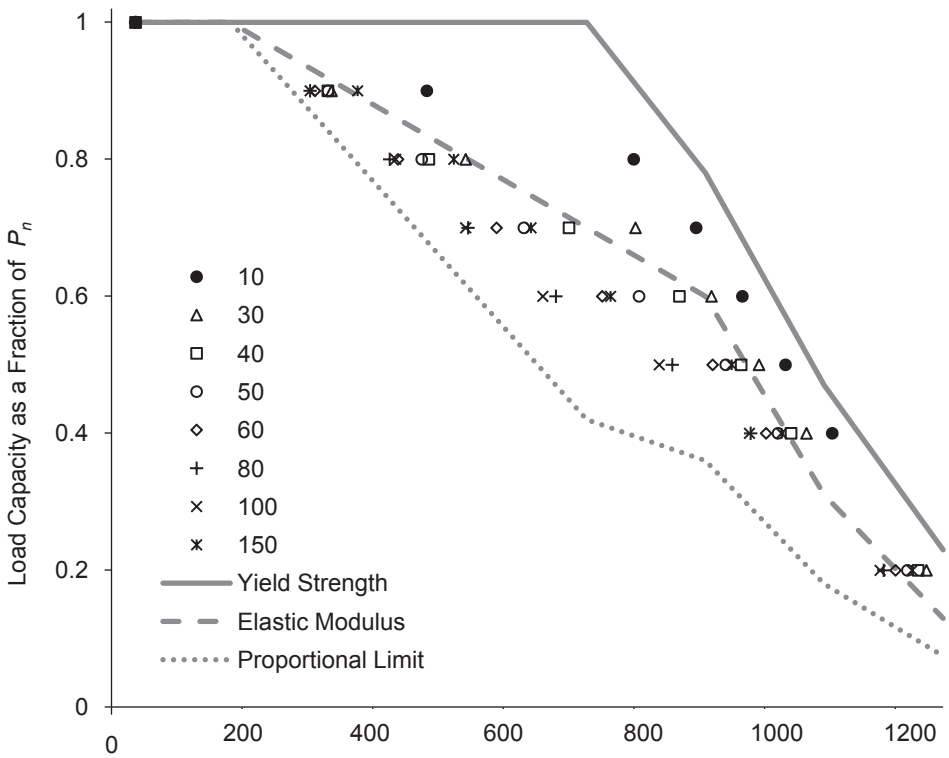

Fig. 6. Change in load capacity due to temperature in W12×58 columns of various slenderness values.

Table 5. Change in Equivalent Material Properties with Temperature								
T (°C) (°F)	20 (68)	100 (212)	200 (392)	300 (572)	400 (752)	500 (932)	600 (1112)	700 (1292)
$(F_y^T/F_y^{20})_{eq}$	1	1	0.89	0.79	0.69	0.56	0.32	0.15
$(E^T/E^{20})_{eq}$	1	1	0.84	0.68	0.54	0.47	0.24	0.098

$$P_n^T = A\left(0.877F_e^T\right), \qquad \text{if } F_e^T \le 0.44F_y^T \tag{2}$$

where

$$F_e^T = \frac{\pi^2 E^T}{\lambda^2} \tag{3}$$

Figures 9a through d compare the various design equations for column capacity at elevated temperatures, including Eurocode 3, AISC 360-05, Takagi and Deierlein, and the proposed method using Equations 1, 2, and 3, along with the results from the analytical parametric studies on W12×58 columns conducted using ABAQUS. Figure 9 shows how the normalized load capacity of columns with different lengths (slenderness values of 30, 50, 80 and 100) change at elevated temperatures. The comparisons in Figure 9 show that the current AISC 360-05 equations with asymptotic bi-linearization of the curvilinear stress-strain-temperature curves are overly unconservative at elevated temperatures. The Takagi and Deierlein, as well as the Eurocode 3, equations provide a good match with analysis results at temperatures greater than or equal to 400 ºC (752 ºF) but are too conservative at lower temperatures. The proposed Equations 1, 2, and 3 used with the equivalent material properties proposed in this study provide a good match with the analysis results at all temperature and slenderness values.

Figures 10a through d show a sampling of the comparisons of column design equations (i.e., axial load capacity versus column slenderness curves) at elevated temperatures from the four methods mentioned earlier. Comparisons are shown for W12×58 at 200 ºC (392 ºF), W8×35 at 400 ºC (752 ºF), W14×159 at 500 ºC (932 ºF) and W14×90 at 600 ºC (1112 ºF). Figure 10 indicates that although the proposed equations compare well with analysis results at all temperature values, they are too conservative for very small slenderness values ($L/r_y < 30$), which are typically uncommon for gravity columns. Therefore, for the purpose of simply supported columns, either of these two methods (Takagi and

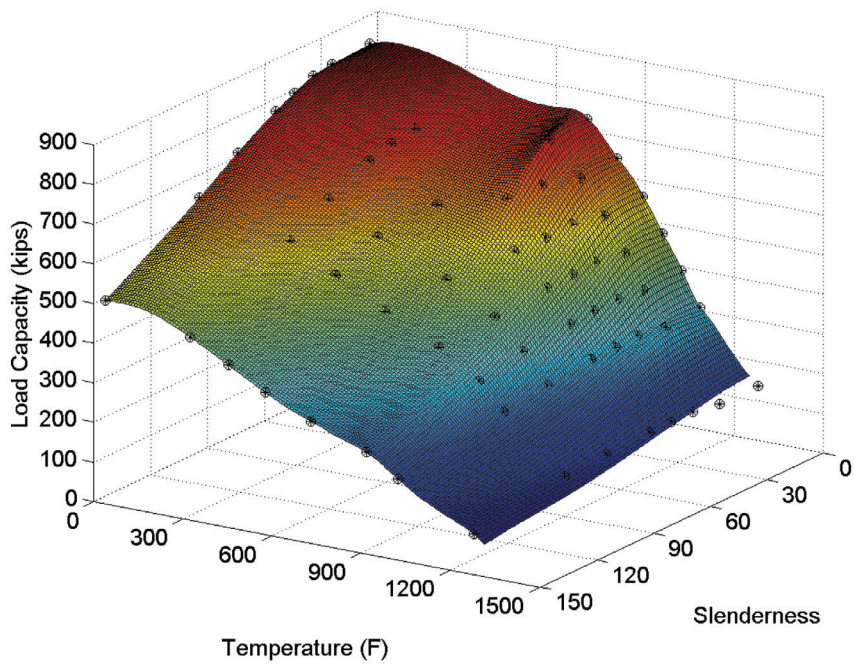

Fig. 7. W12×58: load capacity as a function of temperature and slenderness.

Deierlein or the one proposed in this paper) can be used for designing steel columns at elevated temperatures, as long as their limitations are recognized.

DESIGN EQUATIONS: CONTINUOUS COLUMNS

The design equations presented earlier were limited to columns with simply supported end conditions. This section proposes modifications to the earlier equations to account for the rotational restraints due to continuity with cooler columns above or below. These modifications were developed using the results from the parametric studies conducted on continuous columns. It is important to note that these modifications can be used with any column design methods (i.e., Takagi and Deierlein or the one proposed in this paper).

The results from Tables 3 and 4 were used to develop a three-dimensional surface relating the axial load level (P/P_n) to the slenderness and the failure temperatures similar to the one shown in Figure 7. Column capacity curves corresponding to a particular failure temperature or slenderness can be obtained by taking longitudinal or transverse sections of this three-dimensional surface. Figures 11a through d show the normalized column capacity curves for continuous columns with respect to slenderness at failure temperatures of 400, 500, 600 and 600 ºC (752, 932, 1112 and 1112 ºF). The columns in Figures 11a, b and c are continuous

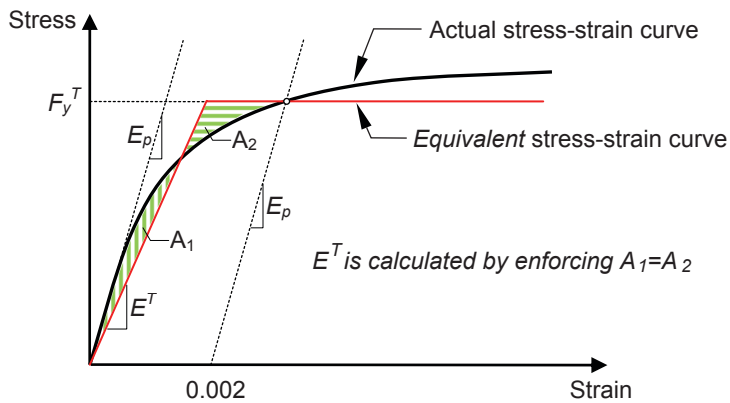

(a)

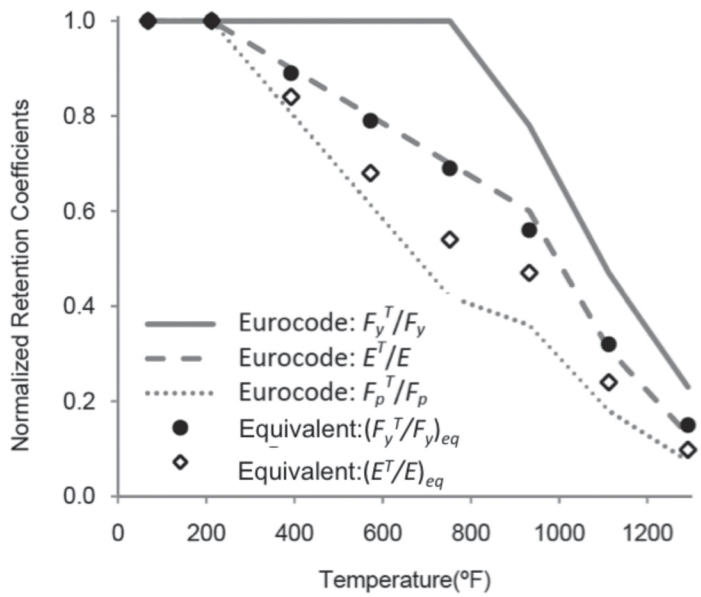

(b)

Fig. 8. (a) Procedure used for bi-linearization of the smooth stress-strain curve; (b) equivalent retention coefficients corresponding to Eurocode guidelines.

at both ends, and the column in Figure 11d is continuous at one end only. These figures also include the corresponding column curves for the simply supported case (without any restraints). Figures 11a, b and c indicate that continuity with cooler columns at both ends significantly improves the axial load capacity of the columns at elevated temperatures. For example, as shown in Figure 11c, at 600 ºC (1112 ºF), the continuous column with slenderness equal to 50 has 40% more axial load capacity than a simply supported column of same length. As shown in Figure 11d, the increase in the load capacity for the W12×58 column continuous at one end only and heated to 600 ºC (1112 ºF) is smaller than the increase for columns continuous at both ends.

The rotational restraints tend to reduce the effective length of the heated column, and this effect can be modeled by using an effective slenderness ratio, λ_{eff}, for the restrained column. The correlation between the actual and the effective slenderness ratios, L/r_y, was developed by using the results from the finite element analyses. This correlation is given in Equation 4. In this equation, T is the temperature of the heated column in ºC; λ is the value of governing slenderness ratio L/r_y, with L being the unbraced length of the column and r_y being the radius of gyration of the section in the governing axis; and λ_{eff} is the effective slenderness of the column.

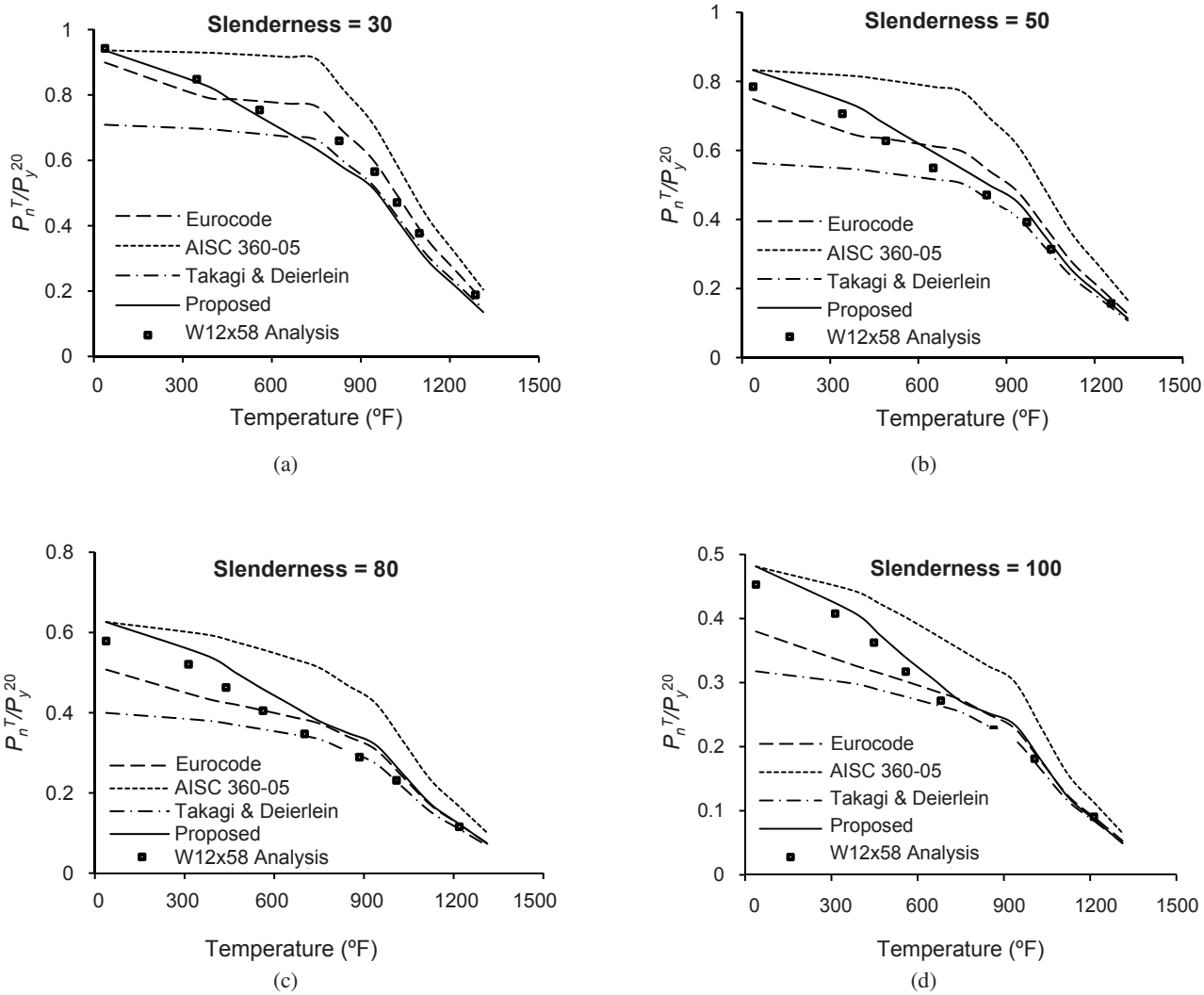

Fig. 9. Comparison of design equations for columns at elevated temperatures with results of the FEM analyses for a W12×58 column section and for $\lambda = L/r_y$ value of (a) 30, (b) 50, (c) 80 and (d) 100.

$$\lambda_{eff} = \begin{cases} \text{if} \quad \lambda \le 10.5: \\ \lambda \\ \text{if} \quad \lambda > 10.5, \text{ and continuous at both ends:} \\ \left(1 - \dfrac{T}{2000}\right)\lambda - \left(\dfrac{35}{2000}\right)T \ge 10.5 \\ \text{if} \quad \lambda > 10.5, \text{ and continuous at one end:} \\ \left(1 - \dfrac{T}{4000}\right)\lambda - \left(\dfrac{35}{4000}\right)T \ge 10.5 \end{cases} \quad (4)$$

Equation 4 has been rewritten as Equation 5 for temperature values in ºF. The correlation for columns continuous at both ends has been illustrated graphically in Figure 12.

$$\lambda_{eff} = \begin{cases} \text{if} \quad \lambda \le 10.5: \\ \lambda \\ \text{if} \quad \lambda > 10.5, \text{ and continuous at both ends:} \\ \left(1 - \dfrac{T-32}{3600}\right)\lambda - \dfrac{35}{3600}(T-32) \ge 10.5 \\ \text{if} \quad \lambda > 10.5, \text{ and continuous at one end:} \\ \left(1 - \dfrac{T-32}{7200}\right)\lambda - \dfrac{35}{7200}(T-32) \ge 10.5 \end{cases} \quad (5)$$

The rotational restraint effects are negligible at ambient temperatures because the columns in the stories above and below are subjected to similar axial load levels and therefore

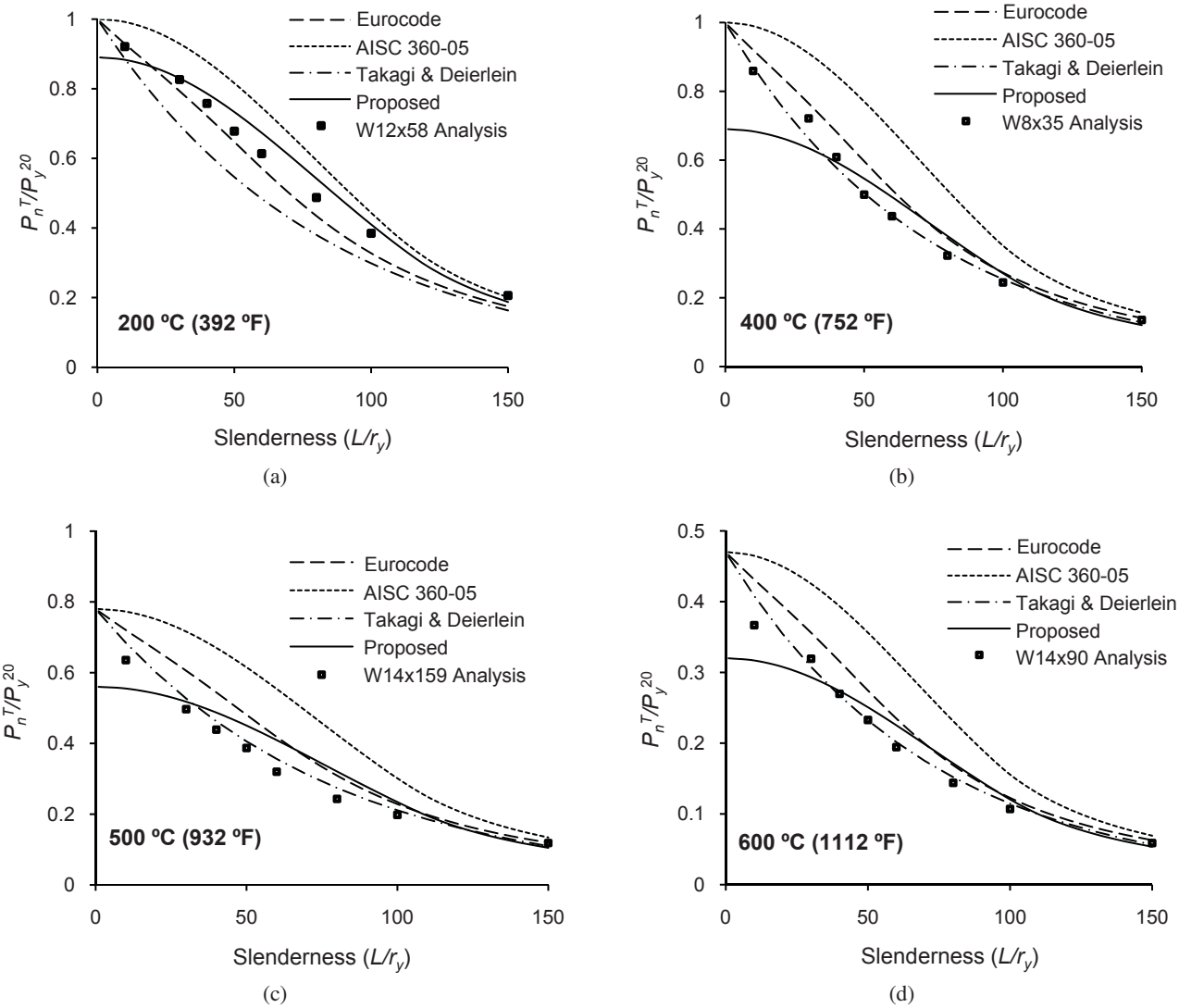

Fig. 10. Comparison of design equations for columns at elevated temperatures with results of the FEM analyses: (a) W12 × 58 at 392 ºF; (b) W8 × 35 at 752 ºF; (c) W14 × 159 at 932 ºF; (d) W14 × 90 at 1112 ºF.

are equally close to their respective stability limits. The effective slenderness values calculated using Equations 4 or 5 can be used with the elevated temperature design equations for simply supported columns to calculate the axial load capacity of rotationally restrained columns. For example, they can be used to modify the proposed column design curves presented in this paper or the one proposed by Takagi and Deierlein. Figure 11 also included the mapping of the continuous column curves to the simply supported column curves by using the proposed correlation between λ and λ_{eff}, the actual and the effective slenderness values. The figure indicates excellent agreement between the column curves predicted using the proposed effective slenderness and those predicted by the finite element analyses.

SUMMARY AND CONCLUSIONS

AISC 360-05 has a new Appendix 4 with provisions to calculate member strength at elevated temperatures. For column strength at elevated temperatures, the appendix provisions recommend the use of flexural-buckling column strength equations at the ambient temperatures with the revised elastic modulus and yield strength values for elevated temperatures. These values represent an asymptotic bi-linearization

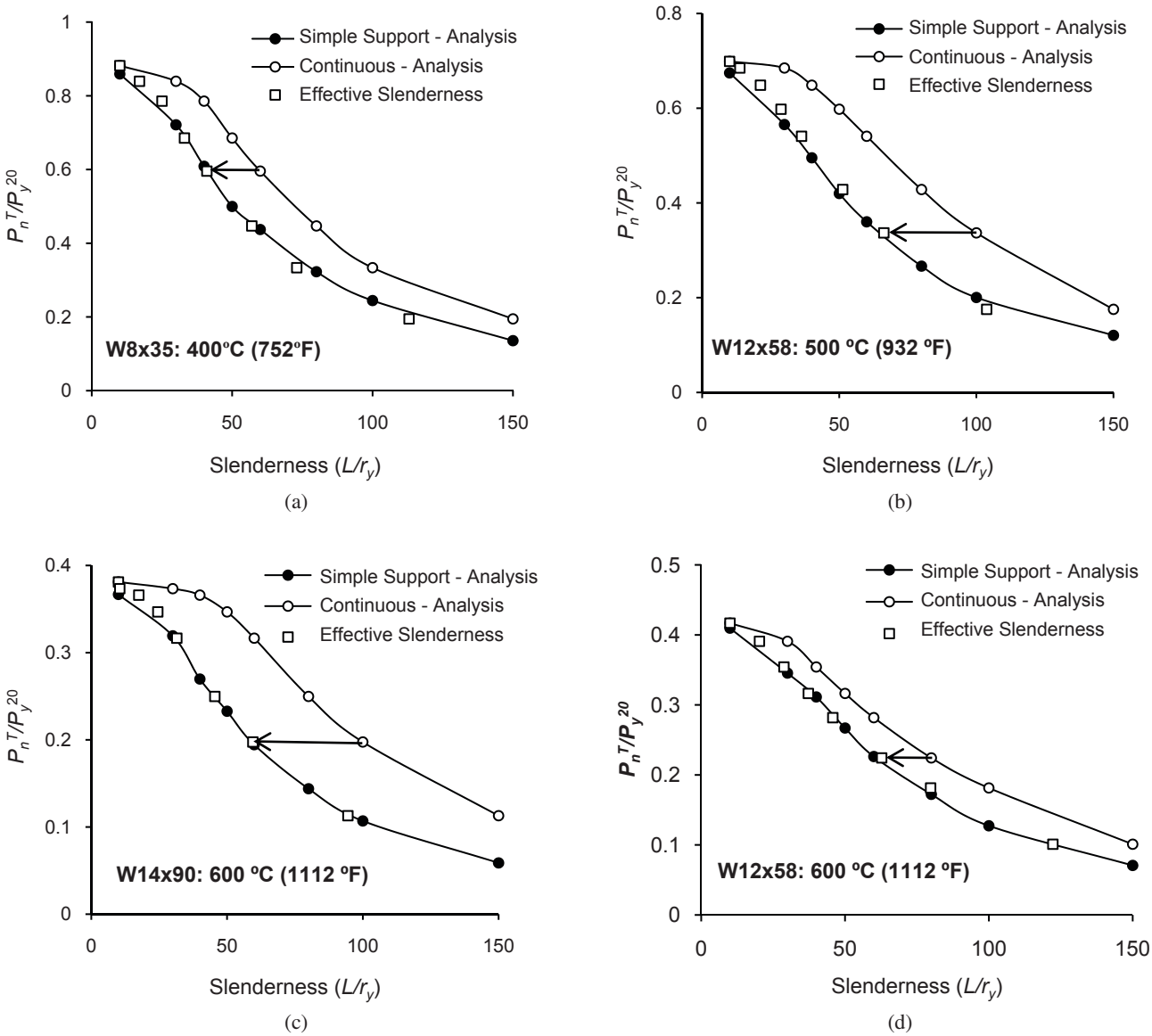

Fig. 11. Comparison of the estimated capacity of columns using the effective slenderness method with the estimated capacity using FEM analysis for (a) W8×35 at 752 ºF, (b) W12×58 at 932 ºF, and (c) W14×90 at 1112 ºF and continuous at both ends; and (d) W12×58 at 1112 ºF and continuous at one end.

of the curvilinear stress-strain-temperature (σ-ε-*T*) curves recommended by Eurocode 3 for structural steel. This asymptotic bi-linearization results in overestimation of the actual stress-strain curve; consequently, the column design equations overestimate the column capacity at elevated temperatures. The column design equations in Eurocode 3 are found to offer much better agreement with the experimental data. Takagi and Deierlein (2007) recommended another equation that has been adopted into the 2010 AISC *Specification*. This equation also has much better agreement with the column capacities estimated by numerical simulations of three-dimensional FEM models. It has a slightly different format and is discontinuous with the AISC column equations at ambient temperatures.

This paper presented the development and validation of analytical techniques for simulating the behavior of wide-flange hot-rolled steel columns at elevated temperatures. Two different modeling approaches using two-noded beam elements and four-noded shell elements were evaluated by comparing analytical results with experimental data. The comparison shows that the detailed models using shell elements offer significantly better accuracy in predicting failure temperature, T_F, of W-shape steel columns. The detailed models include the effects of residual stress and local as well as global geometric imperfections in the member.

The detailed shell element models were used to conduct parametric studies on W-shape hot-rolled steel columns to evaluate the effects of slenderness, load level and different boundary conditions on the failure temperature of the column. The results from the parametric studies were used to evaluate the existing design equations in the literature and to recommend a simple modification to the AISC 360-05 column strength equations at ambient temperatures to make them applicable at elevated temperatures. The study shows that the column capacity at elevated temperatures can be predicted with better accuracy using the ambient AISC column design equations if an improved bi-linear approximation of the steel stress-strain curve is used. The authors provide one such scheme of bi-linearization to determine the values of the equivalent elastic modulus, E^T, and equivalent yield stress, F_y^T, for a given curvilinear stress-strain curve at elevated temperatures. It is observed that the predicted column capacities (or failure temperatures) are in very good agreement with the results of the finite element simulations. Using the existing AISC equations resolves the minor issues of equation format and discontinuity with ambient temperature column capacity equations. More importantly, if a new steel material model is developed or accepted in the near future, the same column design equations can be used by revising the equivalent elastic modulus and yield stress values using the bi-linearization scheme presented in this paper.

The presence of cooler columns above and below has a significant stabilizing effect on heated columns. The axial load capacity of a heated column with cooler columns (above and/or below) is greater than its isolated axial load capacity. Eurocode 3 accounts for this effect by recommending that the effective length of the heated column should be taken as 50 and 70% of the actual length for the cases with cooler columns at both ends and cooler column at one end, respectively. The parametric studies conducted in this paper found that this approach is too simplistic. The effective length reduction depends on the elevated temperature value and the slenderness ratio of the column. Assuming that the columns above and below have the same length and section properties as the heated column, this paper proposed a simple equation that can be used to estimate an effective slenderness for the heated column while accounting for the effects of cooler columns above and below. This equation can be used with any elevated temperature column design approach (existing or new) to account for the stabilization effects from cooler columns.

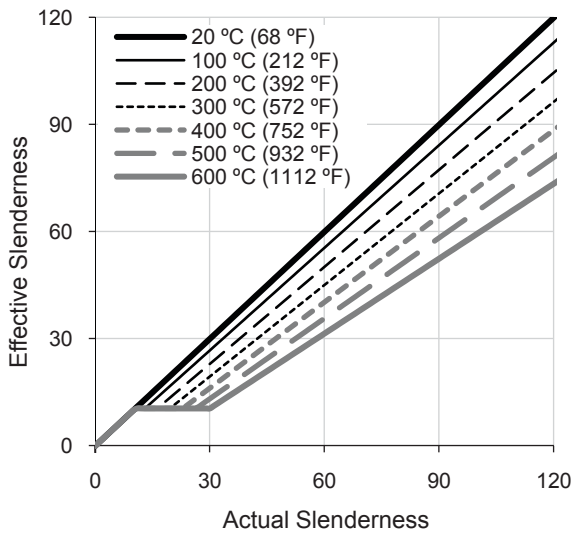

Fig. 12. Proposed relationship between the slenderness of a column continuous at both ends and an equivalent simply supported column.

ACKNOWLEDGMENTS

The research presented in this paper was funded by the National Science Foundation (Grant No. 0601201) and the U.S. Department of Commerce through the Extramural Fire Research Grant Program administered by the National Institute of Standards and Technology, Building and Fire Research Laboratory (NIST-BFRL). Partial funding has also been provided by the American Institute of Steel Construction and the American Iron and Steel Institute. Experimental data, findings and conclusions or recommendations are those of the authors only.

REFERENCES

Aasen, B. (1985), "An Experimental Study on Columns' Behavior at Elevated Temperatures," research report, Division of Steel Structures, Norwegian Institute of Technology, University of Trondheim, Norway.

ABAQUS (2009), *ABAQUS/Standard version 6.9 User's Manuals: Volume I-III*, Hibbitt, Karlsson, and Sorenson Inc., Pawtucket, RI.

AISC (2005a), *Specification for Structural Steel Buildings*, AISC 360-05, American Institute of Steel Construction, Chicago, IL.

AISC (2005b), *Steel Construction Manual*, 13th ed., American Institute of Steel Construction, Chicago, IL.

AISC (2010), *Specification for Structural Steel Buildings*, AISC 360-10, American Institute of Steel Construction, Chicago, IL.

ANSYS (2004), *ANSYS User's Manual*, ANSYS Inc., Canonsburg, PA.

ASCE (2005), *Standard Calculation Methods for Structural Fire Protection*, ASCE/SEI/SFPE 29-05, American Society of Civil Engineers, Reston, VA.

ASTM (2008a), *Standard Methods of Fire Test of Building Construction and Materials*, ASTM E119, American Society of Testing and Materials, West Conshohocken, PA.

ASTM (2008b), *Standard Specification for General Requirements for Rolled Structural Steel Bars, Plates, Shapes, and Sheet Piling*, ASTM A6, American Society of Testing and Materials, West Conshohocken, PA.

Beyler, C., Beitel, J., Iwankiw, N. and Lattimer, B. (2007), *Fire Resistance Testing Needs for Performance-Based Fire Design of Buildings*, National Fire Protection Association, Quincy, MA.

Chen, W.F. and Lui, E.M. (1987), *Structural Stability—Theory and Implementation*, Prentice Hall, Upper Saddle River, NJ.

EN (2005), *Eurocode 3: Design of Steel Structures, Part 1-2: General Rule—Structural Fire Design*, EN 1993-1-2, European Committee for Standardization, Brussels, Belgium.

Franssen, J.M. (2005), "SAFIR: A Thermal/Structural Program for Modeling Structures under Fire," *Engineering Journal*, AISC, Vol. 42, No. 3, pp. 143–155.

Franssen, J.M., Talamona, D., Kruppa, J. and Cajot, L.G. (1998), "Stability of Steel Columns in Case of Fire: Experimental Evaluation," *Journal of Structural Engineering*, ASCE, Vol. 124, No. 2, pp. 158–163.

Hong, S. and Varma, A.H. (2009), "Analytical Modeling of the Standard Fire Behavior of Loaded CFT Columns," *Journal of Constructional Steel Research*, Vol. 65, pp. 54–69.

ICC (2009), *International Building Code*, International Code Council, Falls Church, VA.

Janns, J. and Minne, R. (1981), "Buckling of Steel Columns in Fire Conditions," *Fire Safety Journal*, Vol. 4, No. 4, pp. 227–235.

Lie, T.T. and Almand, K.H. (1990), "A Method to Predict Fire Resistance of Steel Building Columns," *Engineering Journal*, AISC, Vol. 27, No. 4, pp. 158–167.

LS-DYNA (2003), *LS-DYNA Keyword User's Manual V. 970*, Livermore Software Technology Corporation, Livermore, CA.

Neves, I.C., Valente, J.C. and Rodrigues, J.P.C. (2002), "Thermal Restraint and Fire Resistance of Columns," *Fire Safety Journal*, Vol. 37, No. 1, pp. 753–771.

NFPA (2009), *Building Construction and Safety Code*, NFPA 5000, National Fire Protection Association, Quincy, MA.

NIST (2008), *Structural Fire Response and Probable Collapse Sequence of World Trade Center Building 7*, NIST NCSTAR 1-9, National Institute of Standards and Technology, Gaithersburg, MD.

Olesen, F.B. (1980), *Fire Tests on Steel Columns*, Institute of Building Technology and Structural Engineering, Aalborg, Denmark.

Poh, K.W. and Bennetts, I.D. (1995a), "Analysis of Structural Members under Elevated Temperature Conditions," *Journal of Structural Engineering*, ASCE, Vol. 121, No. 4, pp. 664–675.

Poh, K.W. and Bennetts, I.D. (1995b), "Behavior of Steel Columns at Elevated Temperatures," *Journal of Structural Engineering*, ASCE, Vol. 121, No. 4, pp. 676–684.

Rodrigues, J.P.C., Neves, I.C. and Valente, J.C. (2000), "Experimental Research on the Critical Temperature of Compressed Steel Elements with Restrained Thermal Elongation," *Fire Safety Journal*, Vol. 35, No. 2, pp. 77–98.

Ruddy J.L., Marlo, J.P., Loannides, S.A. and Alfawakhiri, F. (2003), *Steel Design Guide 19 Fire Resistance of Structural Steel Framing*, American Institute of Steel Construction, Chicago, IL.

Takagi, J. and Deierlein, G.G. (2007), "Strength Design Criteria for Steel members at Elevated Temperatures," *Journal of Constructional Steel Research*, Vol. 63, No. 8, pp. 1036–1050.

Talamona, D., Franssen, J.M., Schleich, J.B. and Kruppa J. (1997), "Stability of Steel Columns in case of Fire: Numerical Modeling," *Journal of Structural Engineering*, ASCE, Vol. 123, No. 6, pp. 713–720.

Usmani, A. (2005), "Stability of World Trade Center Twin Towers Structural Frame in Multiple Floor Fires," *Journal of Engineering Mechanics*, ASCE, Vol. 131, pp. 654–657.

Valente, J.C. and Neves, I.C. (1999), "Fire Resistance of Steel Columns with Elastically Restrained Axial Elongation and Bending," *Journal of Constructional Steel Research*, Vol. 52, No. 3, pp. 319–331.

Vandamme, M. and Janss, J. (1981), "Buckling of Axially Loaded Steel Columns in Fire Conditions," *IABSE Periodica*, Vol. 3, pp. 81–95.

Varma, A.H., Agarwal. A, Hong, S. and Prasad, K. (2008), "Behavior of Steel Building Structures with Perimeter MRFs under Fire Loading Effects," *Proc. Fifth International Conference: Structures in Fire*, Nanyang Technological University, Singapore, pp. 266–277.

Wang, Y.C. and Davies, J.M. (2003a), "An Experimental Study of Non-sway Loaded and Rotationally Restrained Steel Column Assemblies under Fire Conditions: Analysis of Test Results and Design Calculations," *Journal of Constructional Steel Research*, Vol. 59, No. 3, pp. 291–313.

Wang, Y.C. and Davies, J.M. (2003b), "Fire Tests of Non-sway Loaded and Rotationally Restrained Steel Column Assemblies," *Journal of Constructional Steel Research*, Vol. 59, No. 3), pp. 359–383.

Ziemian, R.D. (2010), *Guide to Stability Design Criteria for Metal Structures*, 6th ed., John Wiley & Sons, New York, NY.